Int. J. Electrochem. Sci., 14 **(2019)** 1116 – 1131, doi: 10.20964/2019.02.05

International Journal of
ELECTROCHEMICAL
SCIENCE
www.electrochemsci.org

Effect of Breakdown Behavior of Passive Films on the Electrochemical Jet Milling of Titanium Alloy TC4 in Sodium Nitrate Solution

Yuanyuan Wang[1] , *Ningsong Qu*[1,2,*]

[1] College of Mechanical and Electrical Engineering, Nanjing University of Aeronautics and Astronautics, Nanjing 210016, China
[2] Jiangsu Key Laboratory of Precision and Micro-Manufacturing Technology, Nanjing 210016, China
[*]E-mail: nsqu@nuaa.edu.cn

Received: 2 August 2018 / *Accepted:* 21 November 2018 / *Published:* 5 January 2019

Electrochemical jet milling (EJM) has broad prospects in engineering applications, its flexibility and versatility offering distinct advantages over traditional electrochemical machining (ECM). In the EJM process, the breakdown time of the passive film plays an important role in the selection of processing parameters. The Ti-6Al-4V (TC4), has been the most widely used titanium alloy in EJM in recent years. However, little research has been conducted on the breakdown time of the passive film on TC4. In this study, experiments concerning the breakdown behavior of the passive film on TC4 were conducted to investigate the influence of breakdown time on machining process in $NaNO_3$ solution. Results showed that the breakdown time of the passive film stabilized at 0.58 s when the current density at the breakdown point exceeded 70 A/cm^2. For any point on the anode surface, the breakdown of the film occurred when the quantity of electric charge reached the point needed for breakdown. The effect of cathode feed rate on the EJM process was also investigated by simulation and experimentation. It was found that an increase of cathode feed rate could improve the machining quality. However, when the feed rate was increased to 50 mm/min, a large area of unbroken passive film remained on the anode surface. Based on systematic studies, a feed rate of between 3 and 12 mm/min was judged to be optimal for the EJM process.

Keywords: Electrochemical jet milling; passive film; TC4 titanium alloy; breakdown behavior; cathode feed rate

1. INTRODUCTION

Ti-6Al-4V (TC4) is the most extensively used titanium alloy in high-end engineering applications, its production in recent years has risen to 50% of all titanium alloys. Titanium and titanium

alloys are known as “space metals” or “marine metals” due to their outstanding characteristics of corrosion resistance and high temperature stability, which has led to a broad applications base in the defense and civil industries. Nevertheless, poor heat conductivity, cutting speed limitations and premature failure of the cutting tools aggravate the difficulties of machining TC4 [1]. Non-traditional processing methods such as electric discharge machining (EDM) and ultrasonic machining (USM) have been used to machine titanium alloys during recent years, however, these methods present certain advantages and drawbacks when used under specific circumstances [2].

Electrochemical machining (ECM) has distinctive features when compared to traditional processing methods. The ECM method has been shown to be unique on account of various processing features, namely, being contactless, no heat-affected-zone, no tool wear, and no residual or thermal stress [3], thus leading to high machining efficiency and reliability. The technology has extensive applications potential in the aeronautics and high-technology fields, as evidenced by the fact that ECM of titanium alloys has become one of the main processing technologies in several countries [4, 5]. In conventional ECM, a pre-shaped cathode is configured to move into the workpiece. The shape of the cathode, however, needs to be altered depending on the shape of the workpiece, which makes the process inconvenient, awkward and time-consuming, especially for the machining of parts with complicated structures [6].

Electrochemical jet milling (EJM) has particular advantages for its flexibility and versatility on machining aviation components or complex-shaped parts due to its use of a hollow tube as the cathode. Much research and development has been performed on EJM over a considerable time with the result that the method has matured, as evidenced by the numerous applications. Natsu [7] investigated the machining characteristics in $NaNO_3$ solution for groove and pitting machining, and confirmed that high current density could improve the surface roughness of the specimen. Vanderauwera [8] investigated the influence of process parameters on the performance of macro electrochemical milling and compared various tubular electrode shapes, multiple passes and step-over to obtain good accuracy. Besides, more and more researchers have found that the passive film formed on the metal surface has great influence on the EJM process.

Electrochemists have been concerned with passivity for almost 200 years [9] and passive film formation has been a subject of much research over the past decade [10-13]. Chin and Mao [14] in their study on mild steel in $NaNO_3$ solution, found that a compact oxide layer formed on the anode surface and was broken down gradually as the anode potential increased. Schultze [11] discussed the growth, reduction, dissolution and modification processes of the passive film and pointed out that the passive film played an important role. In the EJM process on TC4, ultrasonics [15] was explored to assist in the removal of the passive film. To achieve a more stable and controlled removal of the passive film in the machining process, the effects of various electrolytes on the surface finish and material removal rate of TC4 were investigated [16]. Actually, the passive film is a key issue during the EJM process because it is closely related to the metal removal, and the breakdown time of the passive film influences the selection of cathode feed rate. In recent years, the effect of the breakdown time of the passive film on normal dissolution of base metal has been noticed by some researchers. Wang [17], in studies on mild steel in $NaNO_3$ solution, found that the breakdown time could strongly affect metal dissolution. Liu [18] investigated the anodic behavior of TB6 in NaCl solution and revealed the relationship between

breakdown time and current density. However, little research has been conducted on the breakdown of the passive film despite the fact that breakdown of the film has a great influence on the EJM process. This paper aims to investigate the breakdown behavior of TC4 at the anodic interface and to provide a vary selection for the cathode feed rate in the EJM process.

2. EXPERIMENTAL

The electrochemical studies were performed using an electrochemical workstation (Zennium E, Zahner, Germany) with a three-electrod setup, a platinum sheet and a saturated calomel electrode acted as the counter electrode (CE) and reference electrode (RE). The working electrode (WE) was a TC4 square, of which five surface were covered with resin and the remaining surface with an exposed area of 100 mm^2 in the electrolytic cell. The sweep rate was 10 mv/s for an applied voltage of -1 V to 4 V.

The equipment used for testing the breakdown time of the passive film is illustrated in Fig. 1. It was also used to measure the current efficiency of TC4 material. To maintain a constant current density in each run, the dissolution time was controlled precisely using a timer. The TC4 specimens were sectioned (10 × 10 × 10 mm) in order to be embedded in the square groove of the tool holder with the aim of exposing the upper surface only to ensure an equal current density on the machining surface, while the remaining surfaces were insulated with epoxy resin. The cathode could be moved up and down to control the machining gap. The parameters and machining conditions for testing the breakdown time of passive film are summarized in Table 1, while the process parameters for the measuring of current efficiency are summarized in Table 2. Each test was repeated three times.

The schematic of Fig. 2 illustrates the set-up for the EJM of TC4. The major components of the set-up were a power supply (DC), a motion control unit, a filtration system, an electrolytic cell and a monitoring unit. A stainless steel tube with an outer diameter of 1.2 mm and an inner diameter of 0.8 mm served as the cathode. The power supply used had a maximum voltage of 80 V and a maximum current of 40 A. The machining parameters of the grooves in EJM process are summarized in Table 3. All the specimens were rinsed in an ultrasonic bath with acetone and anhydrous ethanol before conducting the experiments.

The data of current with the time during the experiments were recorded by a data recorder (MRR8827; Hioki, Japan). After the experiments, the surface topography of the square specimens and the top-view profiles of the EJM machined grooves were observed using a scanning electron microscope (SEM; S-4800, Hitachi, Japan). The cross-section profiles and surface roughnesses were measured using a 3D Optical Profiler (Sensofar S-neox, Spain). Machining efficiency was evaluated by material removal rate (MRR) which was calculated by:

$$\mathrm{MRR} = \frac{M_L}{t} \qquad (1)$$

where M_L is the experimental weight loss (g), and t is the total machining time (min). The machining accuracy was evaluated by localizability (L_D) which can be expressed by:

$$L_D = \frac{d}{W} \qquad (2)$$

where d is the inner diameter of the cathode and W is the width of the machined groove.

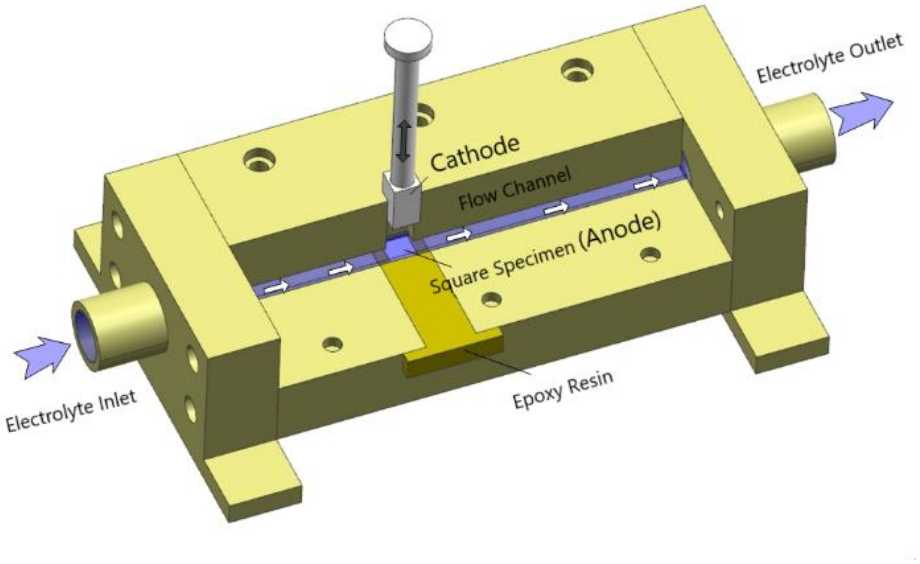

Figure 1. Apparatus for testing the breakdown time of the passive film.

Table 1. Machining conditions for breakdown time tests.

Process parameters	Value
Applied voltage /V	15, 20, 25, 30, 35, 40, 45, 50
Machining gap /mm	0.8
Electrolyte	20% $NaNO_3$ solution
Electrolyte pressure /Mpa	0.5
Electrolyte temperature /^oC	40

Table 2. Machining conditions for current efficiency measurements.

Process parameters	Value
Applied current /A	0.6, 0.8, 1, 1.5, 2, 3, 4, 5, 7, 9, 11, 13
Machining gap /mm	0.8
Electrolyte	20% $NaNO_3$ solution
Electrolyte pressure /Mpa	0.5
Processing area /cm^2	0.25

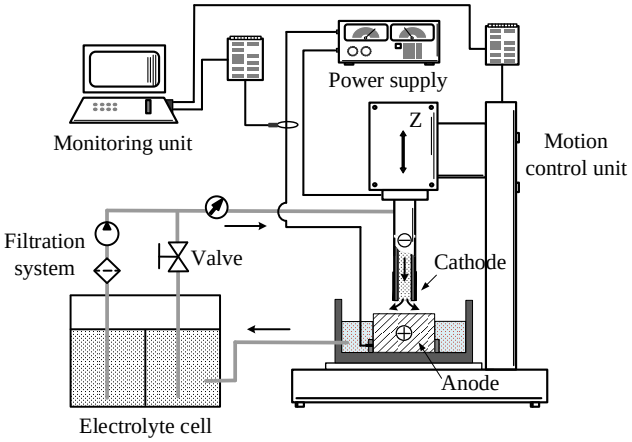

Figure 2. Schematic of the set-up for EJM process.

Table 3. Experiments parameters of grooves in the EJM process.

Index	Value
Applied voltage /V	30
Machining gap /mm	0.3
Cathode feed rate /mm/min	0.8, 1.5, 3, 6, 12, 18
Cathode inner/outer diameter /mm	0.8/1.2
Electrolyte flow rate /L/h	20
Electrolyte temperature /ºC	40

3. RESULTS AND DISCUSION

3.1 Electrochemical characterization of TC4

Titanium has a strong self-passivation ability and the formed passive film on the surface hinders the base metal from dissolving uniformly. The TC4 alloy possesses a Ti content exceeding 85%, which makes the passivation feature a particularly serious and crucial problem in the EJM process [19]. In addition, the dissolution of base metal occurs only after the breakdown of the passive film; therefore, it is essential to acquire a comprehensive appreciation of the electrochemical properties of TC4. Linear sweep voltammetry (LSV) was performed to investigate the polarization characteristics and the obtaining curve is shown in Fig. 3.

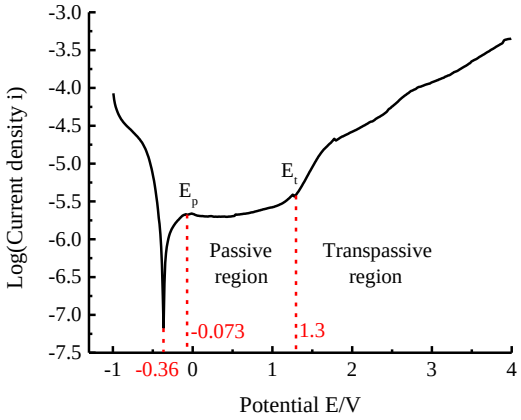

Figure 3. Polarization curve of TC4 in 20% $NaNO_3$ solution. (E_p, E_t are the potentials of the passive and the transpassive regions, respectively.)

It can be clearly observed that the polarization curve is characterized by active dissolution, passivation, and trans-passivation processes. Once the voltage exceeds -0.36 V, the current density increases abruptly and then stops at -0.073V. Within the range -0.073 to 1.3V, the current density remains relatively constant in the passivation region, which is conversant with the natural oxide layer and the formation of the passive film on the surface of the TC4 specimen. This film impedes the normal dissolution of the metal [19, 20]. Once the voltage exceeds 1.3 V, the current density presents a clear trend of increasing, which signifies the breakdown of the passive layer.

3.2 The breakdown behavior of the passive film

The existence of the passive film can protect the non-machined surface to some extent, but it has a negative role for the surface which has to be machined in the EJM process because the dissolution of the base metal occurs only after the breakdown of the passive film. Therefore, it is essential to investigate the breakdown behavior of the passive film.

In ECM process, the constant voltage mode is commonly adopted. In addition, the two electrodes system of tool cathode and workpiece anode are more closer to the actual machining process, so the current density-time curves at different applied voltages are recorded as shown in Fig. 4. The current density shows an increasing trend initially, then the increasing rate begins to slow down due to the formation of the passive film. Subsequently, the current density declines after passing through the inflection point. An increase in the inter-electrode gap due to the removal of the passive film leads to a further decrease of current density. Hence, it is reasonable to consider the inflection point as the breakdown point for the passive film. The decrease in the current density was also regarded as indicating onset of breakdown of the passive film by Wang [17].

From Fig. 4(c), it can be seen that the breakdown of the passive film takes place at about 3.7 s at a voltage of 25 V. The current density reaches 36.37 A/cm^2 and then declines when passing through the breakdown point. The passive film corresponding to the different stages presents different surface conditions. Fig. 5 shows the surface topographies of the specimen at different times (i.e., 1.6 s, 2.47 s and 4.05 s) at the voltage of 25 V. At a machining time of 1.6 s, the specimen surface is still flat and

several localized corrosions occur due to the existence of the passive film as shown in Fig. 5(a); also at this moment the passive film accounts for a high proportion of the surface. As the machining time increases to 2.47 s, the localized corrosion areas increase with only a fraction of the passive film remaining on the surface. More base metal has become exposed to the electrolyte and dissolution occurs, which leads to a rough topography as shown in Fig. 5(b). When the machining time extends to 4.05 s (i.e., exceeding the analytical breakdown time), it can be noticed that the passive film has been basically removed from the surface as shown in Fig. 5(c), but there still exists some uneven dissolution parts or residual reaction products which make the final surface bumpy and lusterless. In general, the specimen surface experiences an unconspicuous dissolution stage initially and shows a shape and flaky texture in the later dissolution. While a honeycomb pit structure was presented on the surface in the early stage and the surface has become more and more rough with the increased dissolving time in NaCl solution in Liu's research [18]. Thus, we consider the variance produced on the surface microcosmic topography may be due to the different properties of the test materials and the electrolytes. The effect of different electrolytes on the surface quality of electrochemical machining was also demonstrated by He [21].

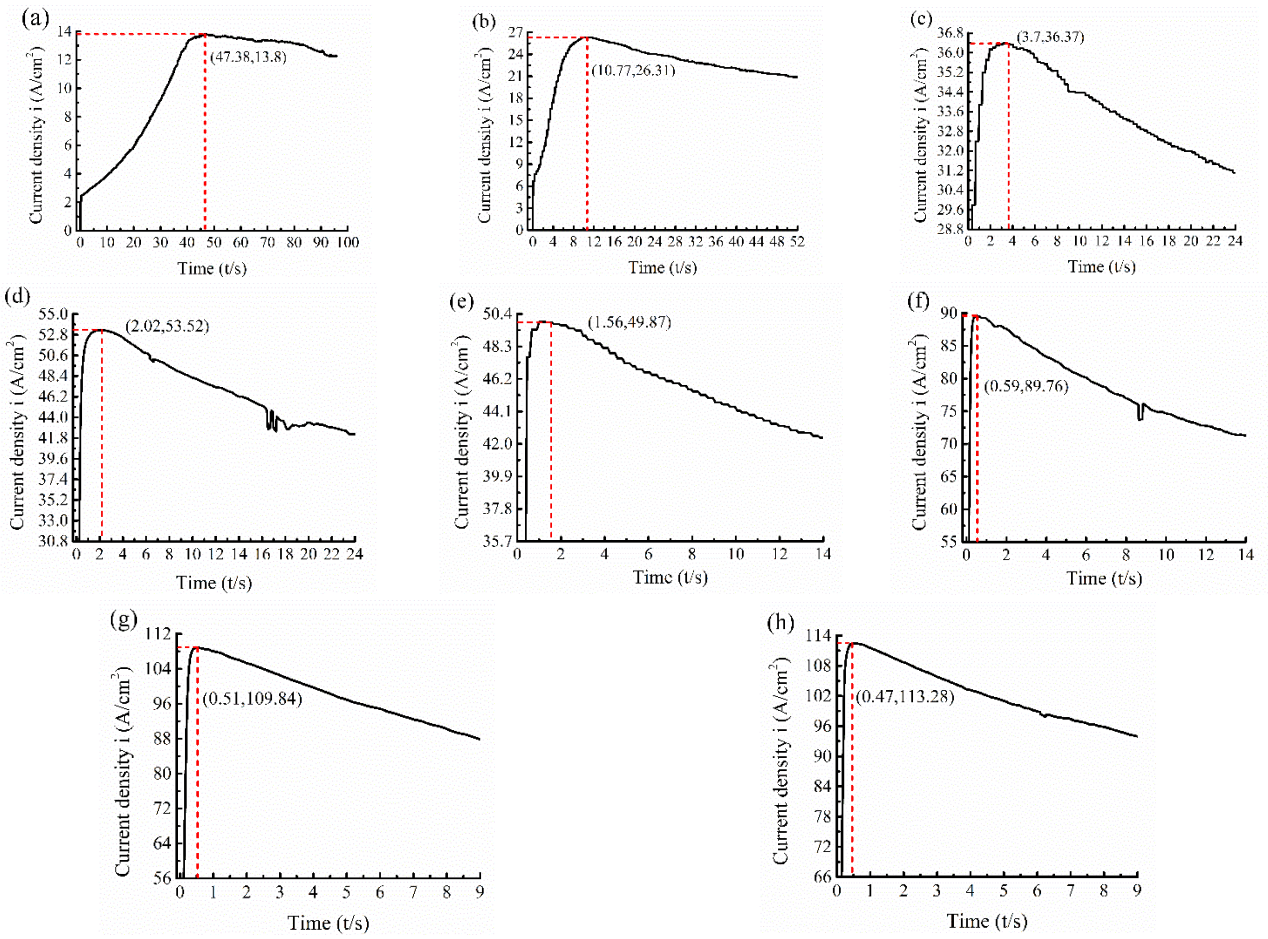

Figure 4. Current density-time curves of TC4 obtained at different voltages: (a) 15 V; (b) 20 V; (c) 25 V; (d) 30 V; (e) 35 V; (f) 40 V; (g) 45 V; (h) 50 V.

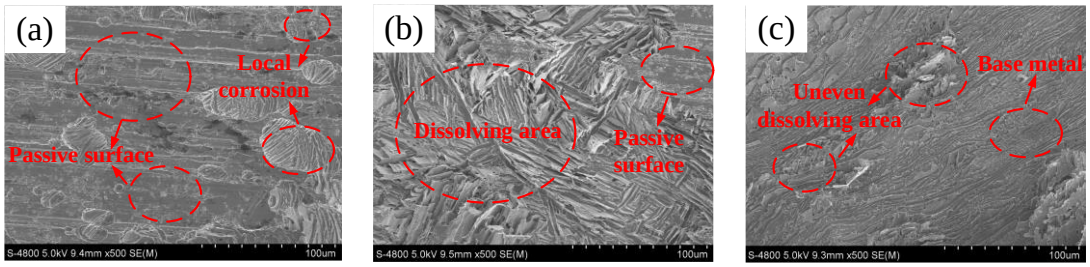

Figure 5. Surface topography of TC4 specimens at different times at 30 V: (a) 1.6 s; (b) 2.47 s; (c) 4.05 s.

From the current density-time curves shown in Fig.4, a relationship between current density and breakdown time of the breakdown point is evident. The breakdown time of the film decreases with increase of current density in the range 10 to 120 A/cm^2, as shown in Fig. 6. At the initial current density of about 13.8 A/cm^2, the breakdown time is up to 47.3 s while the breakdown time is 2.02 s for a current density of 53.5 A/cm^2. Yet, the breakdown time gradually levels off plateauing at about 0.58 s when the current density exceeds 70 A/cm^2. Wang [17], in their investigation of mild steel, also found the similar conclusion that the breakdown time of the passive film reaches a comparatively steady value when the current density exceeds 40 A/cm^2. Though the current density reaches a high value later, the breakdown time is still significant at 1.1 s. Because the thickness of the passive film during anodic polarization is associated with the applied potential, so the different breakdown time of passive film can be derived from different applied voltages [22, 23].

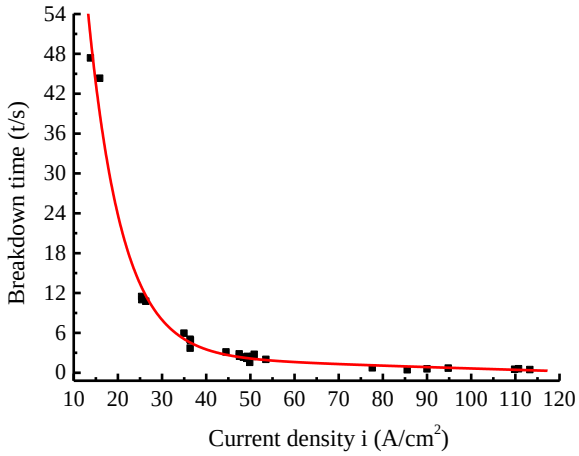

Figure 6. Relationship between current density and breakdown time at the breakdown point.

3.3 EJM simulation and experiments

3.3.1 The simulation and breakdown judgment for a point

To predict the machined shape for the EJM process and compare with the experimental results, a simulation model based on actual structure was set up, as shown in Fig. 7(a). The center of the cathode is in the position of (1.5, 1.5) over the anode surface, then the cathode moves along the x axis with a pre-

designed feed rate. The consequences of simulation of the EJM process are illustrated in Fig. 7(b). The current efficiencies of TC4 in 20% $NaNO_3$ solution are obtained from experimentation and the ηω-current density curve is shown in Fig. 8. The equation for the curve is:

$$\eta\omega = 0.0017 - 0.00114 \times 0.67108^{i} \quad (3)$$

where □ is the current efficiency, □ is the electrochemical volume equivalent ($cm^3/(A{\cdot}min)$) and i is the current density (A/cm^2). The dissolution rate of the anodic workpiece in the normal direction setting in a deformation geometry field can be expressed by:

$$v_n = \eta\omega i \quad (4)$$

The rest of the parameters for the simulation are summarized in Table 4. The results of the simulation are calculated by COMSOL 5.3a software.

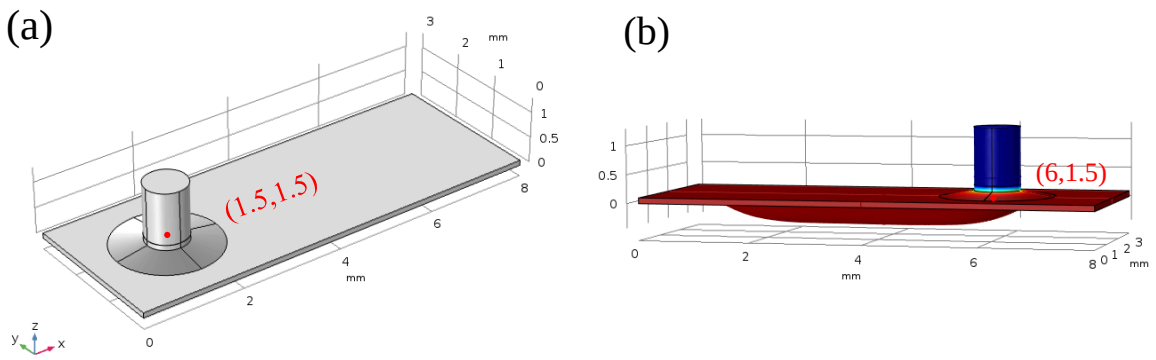

Figure 7. Simulation model for the EJM process: (a) the starting position of the cathode; (b) the machined shape and the final position of the cathode in the simulation for the EJM process.

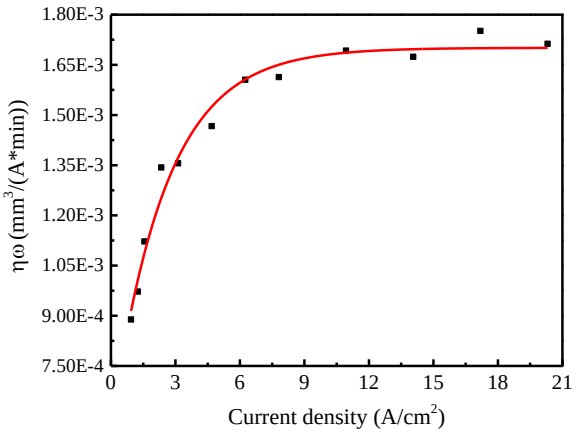

Figure 8. The η**ω**-current density curve of TC4 in 20% $NaNO_3$ solution.

In the practical EJM process, the cathode is fed over the anode surface continuously and this causes a drastic change in the distribution of electric fields. For any point on the anode surface, the current density changes with the time. Therefore, an equivalent charging process of the passive layer capacitor is introduced to describe the breakdown of the passive layer [16, 18, 19]. The electric charge can be calculated from the integration of time and current density:

$$Q = \int_0^{t_b} i dt \quad (5)$$

where t_b is the corresponding breakdown time for the breakdown point. Fig. 9 shows the relationship between the electric charge Q and the current density of breakdown point. It can be observed that the electric charge decreases with increase of current density. The electric charge required for the breakdown of the passive film is different for different current densities with high electric charge being needed for breakdown at low current density.

Table 4. Simulation parameters for the EJM model.

Index	Value
Applied voltage /V	30
Machining gap /mm	0.3
Cathode feed rate /mm/min	0.8, 1.5, 3, 6, 12, 18
Feeding length /mm	4.5
Conductivity of electrolyte /S/m	19.2
Electrolyte temperature /ºC	40

In investigating the anodic dissolution behavior of TB6, Liu [18] reported Q to be a constant material property and an indicator of base metal dissolution. One of the factors leading to the difference in electric charge is probably related to the properties of the material. TC4 is different from TB6 in terms of matrix structure and has a higher Ti content than TB6, which makes the breakdown behavior of TC4 have a stronger association with current density. Another factor may be connected to the nature of the electrolyte. The active Cl^- and passive NO_3^- ions produce opposite effect and lead to the inconsistency of the electric charge Q.

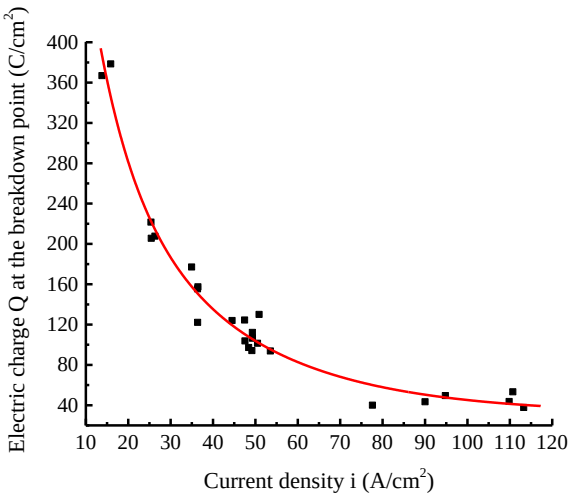

Figure 9. Electric charge-current density curve of the breakdown points from the experiments.

The value of the electric charge Q plays a critical role in evaluating whether the breakdown of the passive film at a point occurs on the surface in the simulation. In this section, point A (4, 1.5, 0) of

Fig. 10 is taken as an example; the cathode feed rate was 1.5 mm/min with a voltage of 30 V. The current density-time curve of point A from the simulation demonstrates initially an increasing trend and later a decrease as shown in Fig. 11(a). The electric charge quantity Q_{t0} of point A at any time t_0 calculated by the integration of current density and time undergoes a steady growth and finally reaches a nearly constant value, namely, the total electrical charge. According to a previous analysis, breakdown of the passive film occurs at any point on the anode surface and the base metal, which performs normal electrochemical dissolution, can be determined by comparing the values of Q_{t0} and Q.

Fig. 11(b) shows the electric charge quantity Q_{t0}-current density curve of point A and the electric charge Q-current density curve of the breakdown point (refer to Fig. 9), where it can be seen that the two curves intersect at point B and the value of Q_{t0} is greater than the value of Q beyond point B. The ordinate value of point B, namely, the amount of electric charge needed for breakdown of the passive film at point A is 170.38 C/cm^2. Then the corresponding time for breakdown of the passive film at point A to occur can be obtained from Fig. 11(a). At 75.26 s, the passive film at point A has been removed because the electric charge needed for breakdown of the passive film has been attained, though the center of the cathode is at a distance of 0.618 mm away from point A. After 75.26 s, the remaining electric charge (i.e., the total of the quantity of electric charge minus the electric charge Q_b), which is all used for the dissolution of base metal, is accompanied by an increase of current density. The position of point A in the electric field changed from the marginal area to the center and then away from the center with a decrease in current density. In addition, the current density is restricted within the jet, so the current density is highly concentrated in the center [24, 25]. Thus we can infer that the electric charge quantity Q_{AY} (calculated by the integration of current density and time) of a point on the surface from point A along the Y axis is gradually reduced.

The breakdown time for the passive film of point A is from the start of current flow to the occurrence of breakdown, so the breakdown time for point A at 1.5 mm/min is about 20.3 s. Similarly, for any point on the anode surface once the breakdown of the passive film occurs then the breakdown time can be inferred.

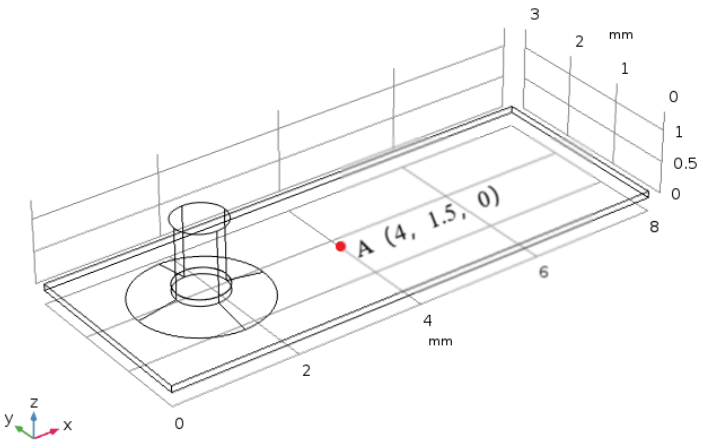

Figure 10. Position of point A on the processing path in the simulation model.

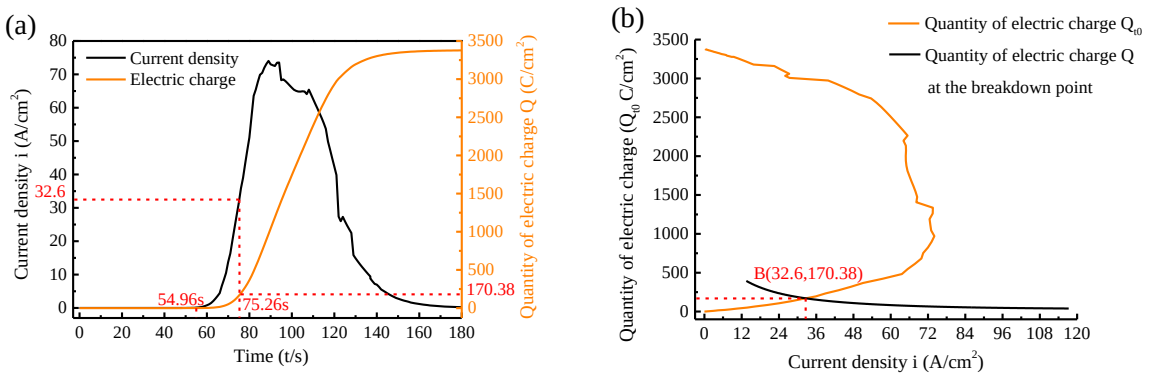

Figure 11. Simulation condition for point A: (a) distribution of current density and electric charge with time in the EJM process at 1.5 mm/min; (b) comparison diagram of the quantity of electric charge Q_{t0} and Q_b.

3.3.2 Effect of cathode feed rate on EJM

To investigate the influence of the cathode feed rate on the EJM process, an experiment and a simulation were conducted. The processing parameters were summarized in Table 3 and Table 4 which shown above. At a voltage of 30 V, the top-view profiles of the machined grooves obtained under selected feed rates with a machining length of 10 mm are presented in Fig. 12. Fig. 13 shows the cross-section profiles obtained from the simulation and the experimental results.

From inspection of Fig. 12(a) to (f) and Fig. 13, it can be seen that the groove depth is inversely proportional to the cathode feed rate. The width and trace left on the surface became narrow and shallow with increase of feed rate. Fig. 12(d) to (f) indicate that the decreasing trend of the groove width is slowing down, even though the feed rate is still increasing because the minimum groove width is limited by the inner diameter of the tube electrode. Moreover, it can be noticed that the surface of the groove at the bottom presents sparse and flaky from the enlarged view in Fig. 12(f) which is similar to the surface topography in Fig. 5(b), and the stray corrosion on both sided of the groove is also serious. The grooves generating in the simulation were larger than the experimental results because the time for breakdown of the passive film was not considered in the simulation.

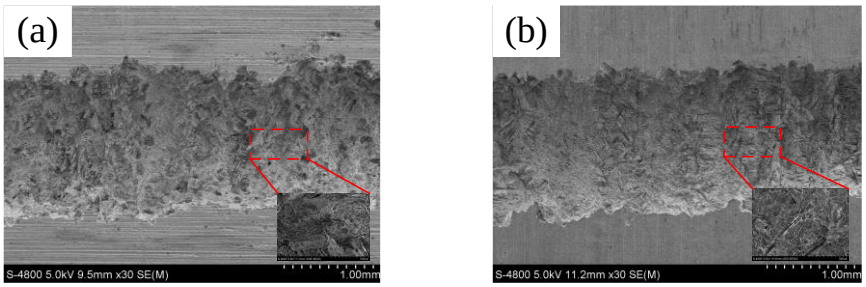

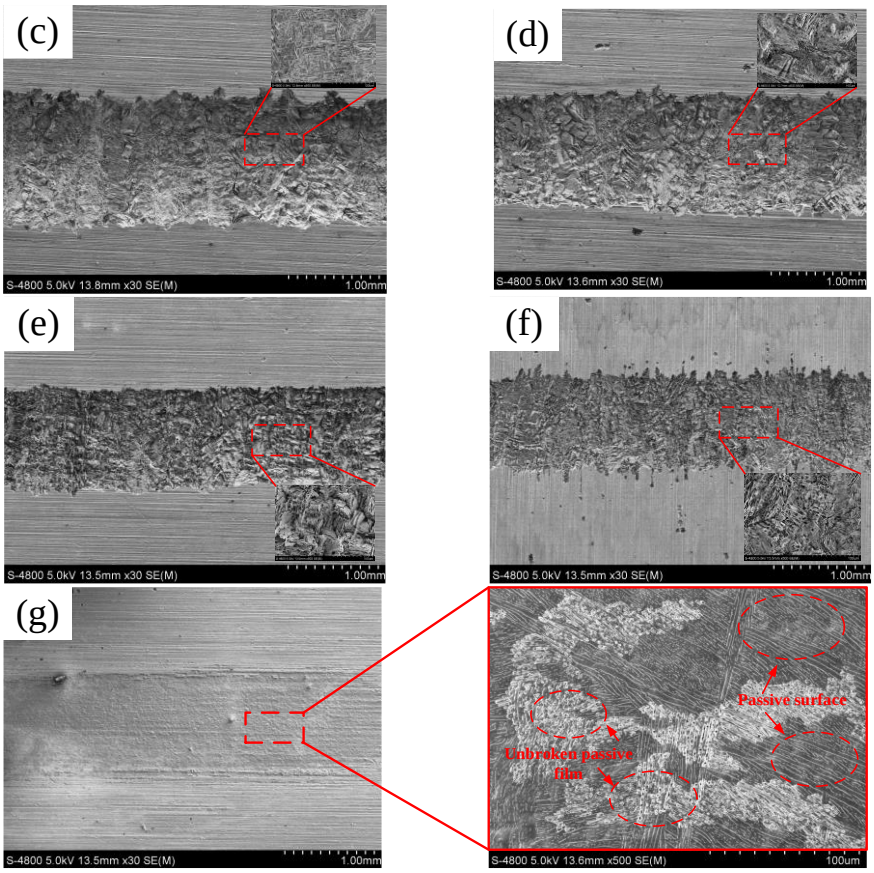

Figure 12. Surface topographies of grooves obtained for experiments at selected feed rates: (a) 0.8 mm/min; (b) 1.5 mm/min; (c) 3 mm/min; (d) 6 mm/min; (e) 12 mm/min; (f) 18 mm/min; (g) 50 mm/min.

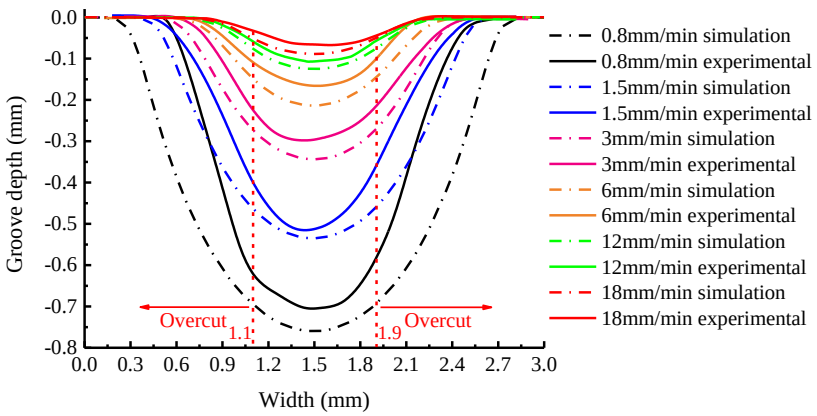

Figure 13. Comparison chart of the cross-section profiles of simulation and experimental results.

Fig. 14 demonstrates the corresponding current density, electric charge and breakdown time for point A at the moment of breakdown for the passive film with the selected feed rates in the simulation. It may be observed that the current density at point A increased, while the electric charge needed for the breakdown of the passive film and the breakdown time decreased with increasing feed rate. The breakdown of the passive film at point A took place when the current density was increasing and the

electric charge reached the amount needed for breakdown. It can be noticed that the breakdown time was shortened from 35.61 s at 0.8 mm/min to 2.27 s at 18 mm/min. The faster the feed rate, the shorter time it takes for the tubular cathode to move to point A, which result the formation and growth time for the passive film of point A shortens and the electric charge needed for the breakdown of passive film decreases. Jiang reported that the increase of film thickness and film resistance of stainless steel follows the direct logarithmic law with time [26], and Schroeder also indicated that the thickness of passive film on titanium alloy varies with the time [27].

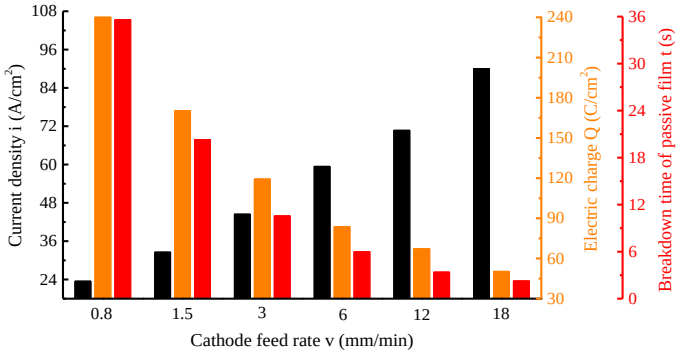

Figure 14. Breakdown condition of point A at the selected feed rates.

To assess the effect of cathode feed rate on the quality of machining by EJM, three performance indexes were evaluated. The surface roughness was used to measure the bottom quality of the machined grooves, while the machining efficiency and machining accuracy were evaluated by MRR and localizability. The results, shown in Fig. 15, illustrate that a fast feed rate can enhance machining accuracy owing to the improvement of the localizability. High localizability means that the width of the machined groove approaches the inner diameter of the cathode with a small overcut being obtained. Fig. 13 also confirms this finding. The MRR increases with an increase of feed rate due to the increase of current density, though the value for the MRR is small owing to the small inner diameter of the tubular cathode. The surface roughness also improved as the current density increased. N. Schubert et al. also verified that high current density would help to obtain a smooth surface in their investigation on the mechanism of anodic dissolution [28]. However, when the feed rate rose to 50 mm/min, the electric charge was insufficient for breakdown of the film. The topography of the specimen surface indicated large proportions of unbroken passive film had remained, as shown in Fig. 12(g), and nearly no processing trace has been left from the macro perspective. The grooves obtained through jet ECM by Liu also demonstrated similar processing results, namely the small width and depth of groove produced at the high cathode feed rate, accompanied by the unbroken passive film and undissolved metal base [29].

In conclusion, to achieve a superior and comprehensive machining performance in EJM of TC4, optimization of the cathode feed rate is recommended; a cathode feed rate of 3 to 12 mm/min was judged to be optimal in this work.

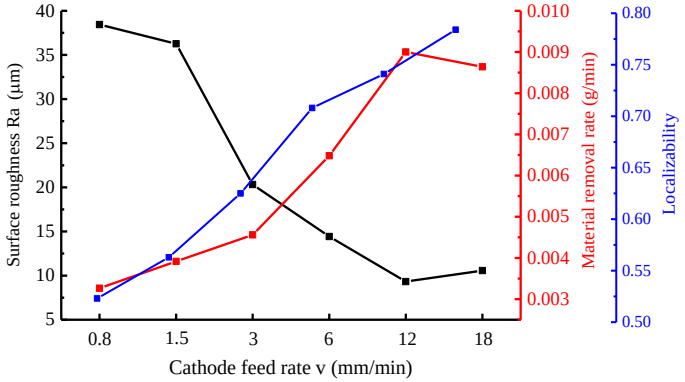

Figure 15. Effect of evaluation indexes on machining quality at the selected feed rate in EJM process.

4. CONCLUSIONS

The paper has focused on the effects of breakdown time of the passive film on the anodic interface of TC4 in $NaNO_3$ solution. Based on experiments, the electric charge at the breakdown point was used to provide a basis for the selection of cathode feed rate. In addition, the effect of cathode feed rate on the EJM process was also investigated. The conclusions can be summarized as follows:

(1) The relationship between current density and breakdown time of the breakdown point shows that a higher current density requires a shorter time for the breakdown of passive film with current densities ranging from 10 to 120 A/cm^2. When the current density exceeded 70 A/cm^2, the breakdown time became stable and remained constant at about 0.58 s.

(2) The electric charge for the breakdown of the passive film at any point on the anode surface was different at the different current densities, and high electric charge was needed for breakdown at low current densities.

(3) A fast cathode feed rate can improve the machining quality in the EJM process, and if the feed rate increases to 50 mm/min, the dissolution of base metal hardly occurs with a large area of passive film remaining on the surface. So, a feed rate of 3 to 12 mm/min was judged to be optimal and appropriate for industrial application.

ACKNOWLEDGEMENT
This work was supported by National Key Research and Development Program of China (2018YFB1105902).

References

1. M. D. Moses and M. P. Jahan, *Int. J. Adv. Man. Tech.,* 81 (2015) 1345.
2. S. S. Anasane and B. Bhattacharyya, *Int. J. Adv. Man. Tech.,* 86 (2016) 1.
3. M. S. Hewidy, S. J. Ebeid, T. A. EI-Taweel and A. H. Youssef, *J. Mat. Process. Tech.,* 189 (2007) 466.

4. G. V. Smirnov, N. D. Pronichev, M. V. Nekhoroshev and V. I. Bogdanovich, *Mater. Sci. Eng.,* 177 (2017) 1.
5. A. D. Davydov, T. B. Kabanova and V. M. Volgin, *Russian. J. Electrochem.,* 53 (2017) 941.
6. T. Kurita and M. Hattori, *Int. J. Mach. Tool. Manu.,* 46 (2006) 1804.
7. W. Natsu, T. Ikeda and M. Kunieda, *Precision. Eng.,* 31 (2007) 33.
8. W. Vanderauwera, M. Vanloffelt, R. Perez and B. Lauwers, *Procedia. Cirp.,* 6 (2013) 356.
9. R. P. Frankenthal and J. Kruger, *Corros. Sci.,* 7 (1978) 341.
10. D. D. Macdonald, *Pure. Appl. Chem.,* 71 (1999) 951.
11. J. W. Schultze and M. M. Lohrengel, *Electrochim. Acta.,* 45 (2000) 2499.
12. P. Schmuki, *J. Solid. State. Electrochem.,* 6 (2002) 145.
13. C. O. A. Olsson and D. Landolt, *Electrochim. Acta.,* 48 (2003) 1093.
14. D. T. Chin and K. W. Mao, *J. Appl. Electrochem.,* 4 (1974) 155.
15. J. Mitchell-Smith and A. T. Clare, *Procedia. Cirp,* 42 (2016) 379.
16. A. Speidel, J. Mitchell-Smith, D. A. Walsh, M. Hirsch and A. Clare, *Procedia. Cirp.,* 42 (2016) 367.
17. D. Y. Wang, Z. W. Zhu, B. He, Y. C. Ge and D. Zhu, *J. Mat. Process. Tech.,* 239 (2017) 251.
18. W. D. Liu, S. S. Ao, Y. Li, Z. M. Liu and H. Zhang, *Electrochim. Acta.,* 233 (2017) 190.
19. M. Weinmann, M. Stolpe, O. Weber, R. Busch and H. Natter, *J. Solid. State. Electrochem.,* 19 (2015) 485.
20. J. Pouilleau, D. Devilliers, F. Garrido, S. Durand-Vidal and E. Mahe, *Mater. Sci & Eng. B.,* 47 (1997) 235.
21. Y. F. He, H. X. Xiao, W. M. Gan, Q. Yu and F. H. Yin, *Procedia. Cirp,* 68 (2018) 751.
22. A. Veluchamy, D. Sherwood, B. Emmanuel and I. S Cole, *J. Electroanal. Chem.,* 785 (2017) 196.
23. A. H. Heuer, H. Kahn, F. Ernst, G. M. Michal and D. B. Hovis, *Acta Mater.,* 60 (2012) 716.
24. J. Mitchell-Smith, A. Speidel and A. T. Clare, *J. Manu. Process.,* 31 (2018) 273.
25. T. Kawanaka and M. Kunieda, *CIRP. Ann-Man. Tech.,* 64 (2015) 237.
26. R. J. Jiang, Y. W. Wang, X. Wen, C. F. Chen and J. M. Zhao, *Appl. Surf. Sci.,* 412 (2017) 214.
27. V. Schroeder, *J. Biomed. Mater. Res A.,* 90 (2009) 1.
28. N. Schubert, M. Schneider and A. Michealis, *Electrochim. Acta.,* 113 (2013) 748.
29. W. D. Liu, S. S. Ao, Y. Li, Z. M. Liu, Z. M. Wang and Z. Luo, *Int. J. Adv. Man. Tech.,* 90 (2017) 2397.